# Influence of Tars on the Maximum Hydrogen Utilization in SOFCs with Biogeneous Gases

**Martin Hauth[1], Nadine Frank[2], Jürgen Karl[1]**
[1] Institute of Thermal Engineering, Graz University of Technology
Inffeldgasse 25/B
AUT-8010 Graz / Austria
Tel.: +43-316-873-7319
Fax: +43-316-873-7305
martin.hauth@tugraz.at

[2] Institute of Energy Systems, Technical University of Munich
Boltzmannstraße 15
GER-85747 Garching / Germany
Tel.: +49-89-289-16272
Fax: +49-89-289-16271
frank.nadine@swm.de

## Abstract

A SOFC system with integrated biomass gasification is a promising technology to achieve high electrical and thermal efficencies for decentralized power generation [20]. This system requires a gas cleaning unit due to impurities in the wood gas to avoid degradation of the Ni-anode. In the case of a hot gas cleaning unit a reformer may be used to convert tars and thus decrease the tar concentration at the anode entry to a very low level. Another possible option would be the direct utilisation or reforming of hydrocarbons at the anode. Wood gas from an allothermal steam gasifier contains sufficient water to allow a complete reforming of the hydrocarbons present in the biogeneous gas. The internal reforming of methane in the SOFC is commonly known [21]. Tests with real woodgas using no pre-reformer in the gas cleaning unit have resulted in no significant degradation of the anode, underlining the apparent insensitivity of the SOFC against tars [3]. Experiments with several synthetic tars at a constant current density identified certain tar species to act as fuel whereas the presence of other tar species significantly decreased the cell voltage due to the inhibition of methane reforming [4]. The electrochemical conversion of methane significantly reduces for naphthalene containing synthetic wood gases [19]. Due to the temperature dependency of the conversion of hydrocarbons less methane and tars respectively are being reformed at lower temperatures leading to lower hydrogen partial pressures, higher hydrogen utilizations and higher degradation rates of the fuel cell. High hydrogen utilizations may cause oxidation of the anode. This paper presents calculations with FactSage of tar laden syngases present at the anode accounting the individual temperature ranges and $H_2O$ contents of tar reforming. The calculated produced amount of $H_2$ and CO due to reforming which is electrochemically converted defines the allowable hydrogen utilization for a certain current density. The calculations are based on gas concentrations as obtained from an allothermal steam gasifier thus using a steam-to-carbon ratio above the critical value for carbon formation. These calculations are expected to enable the predection of a temperature-current density matrix for the maximum tar content allowed in order to reach a maximum hydrogen utilization of 85%. Vice versa it will be possible to predict a maximum possible hydrogen utilization with gas from a certain gasifier type in order to prevent degradation rates of fuel cell stacks operated on biogeneous gas. The calculation model is intended to be a basis for future single cell tests.

# Introduction

Solid Oxide Fuel Cells (SOFC) are a promising technology for decentralized power generation. Their capability of converting CO and $CH_4$ and their robustness against impurities of the fuel gas compared to low temperature fuel cells facilitates the use of producer gas from biomass gasification [12]. Studies have shown that SOFC systems with integrated biomass gasification provide high electrical efficiencies above 50% [1]. The producer gas contains impurities such as particles, tars, sulphur compounds, alkali, heavy metals and ammoniac ([2], [3]). Gas Cleaning Units divided according to their working temperature are used to reduce the impurities to very low levels [3]. Thermodynamically hot gas cleaning units are preferable to avoid a heat sink between gasifier and SOFC. Tests with real wood gas have resulted in no significant degradation of the anode, underlining the apparent insensitivity of the SOFC against tars [3]. Thereby a medium temperature gas cleaning unit with a by-passed pre-reformer was used leading to high tar levels entering the anode chamber. The direct conversion of the higher hydrocarbons and therefore using the high energy contents as well as the simplification of the gas cleaning unit increases the efficiency. The multitude of tars present in the producer gas do not allow the explanation of specific degradation mechanisms of the anode due to the individual behaviour of each sort of tar. Experiments with several synthetic tars at a constant current density identified certain tar species to act as fuel whereas the presence of other tar species significantly decreased the cell voltage due to the inhibition of methane reforming [4]. Due to the Ni-containing anode and the steam content of the fuel gas reforming is favored converting the hydrocarbons to $H_2$ and CO. Dry fuel gas containing hydrocarbons promote carbon deposition at high temperatures ([4], [6]) Thus a certain steam-to-carbon ratio is necessary to prevent coke formation on the anode surface causing cell degradation ([5], [7], [9])

The exact reforming reaction mechanisms at the anode are still unclear. Heterogeneous catalysis models suggest adsorption of the hydrocarbons on the Ni surface, decomposition, surface reaction and desorption of the products from the Ni surface [11]. Products may be $H_2$ and CO which only then get electrochemically converted [10]. Kinetic inhibition due to the many steps of the reforming reaction can lead to a decreasing reactive surface caused by the adsorption on the Ni particle. Overall yields from the reforming of a fuel mixture are not additive of yields from individual fuel components, rather the more reactive component is consumed first [12].

Steam reforming tests have been done with methane [10], methanol, ethanol ([6], [10]), octane, 2,2,4-trimethylpentane, formic acid, acetic acid, butyric acid [6], propane ([6], [7]) and ethane [7]. The reforming behaviour of the so called tars (hydrocarbons higher than $C_6$ [16]) on Ni-catlalysts were investigated for benzene, toluene, naphthalene in ([13], [14], [15]). V-I polarization curves of the direct use of undiluted n-decane as well as the influence of steam on carbon deposition using n-butane as fuel is investigated in [8].

Assuming that only the reforming products such as $H_2$ and CO contribute to the cell voltage explains the reduction of the cell voltage due to incomplete or inhibited conversion depending on the exact reaction mechanisms. Measurements of the cell voltage during the direct use of acethylene, ethylene, toluene, naphthalene, phenanthrene and pyren were performed in [4]. Incomplete or inhibited conversion results in less produced $H_2$ and CO. This means a lower Nernst voltage and for a constant current density an increase of the hydrogen and carbon monoxide utilization causing a voltage drop due to concentration

polarization. Consequently the partial pressure of the oxygen increases causing cell degradation by Ni-oxidation of the anode.

The tar content increases the Nernst voltage only in case that the tars are converted into $H_2$ and CO. In reality reforming occurs only at high temperatures. Figure 1 shows the catalytic conversion rate of naphthalene on a nickel catalyst depending on the temperature.

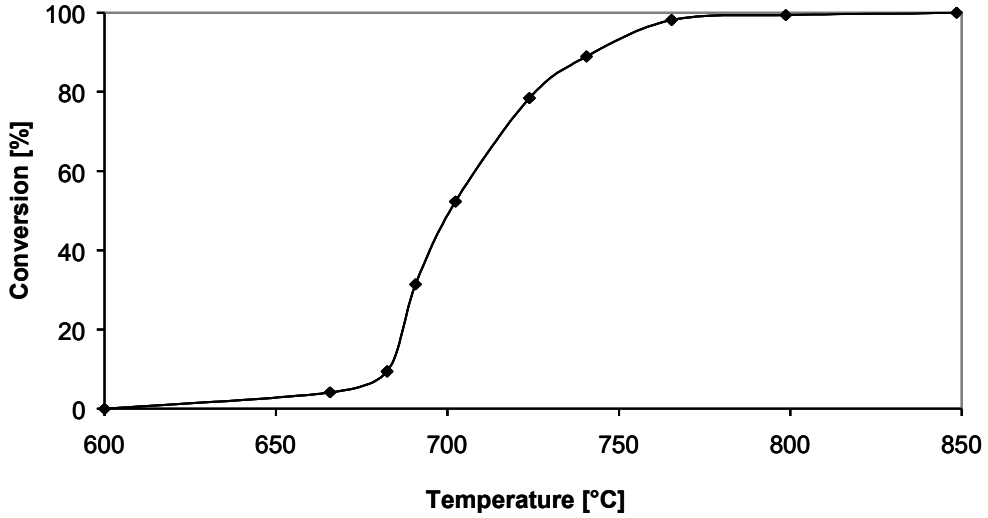


*Figure 1: Catalytic Conversion of naphthalene in the presence of $H_2$ and $H_2O$ [13]*

The temperature depending conversion rate of the reforming of naphthalene on a Nickel catalyst investigated in [13] was used to calculate the Open Current Voltage (OCV) in [19]. Figure 2 shows the curves for a producer gas with 1500ppm naphthalene. The upper dotted curve represents the OCV for equilibrium. This happens in the case that all the naphthalene gets reformed. The bottom dotted curve assumes 0% reforming. Presuming the naphthalene to convert depending on the temperature the OCV amounts according the full curve in figure 2. In doing so only a part of the naphthalene gets reformed at low temperatures whereas the rest is considered to be inert.

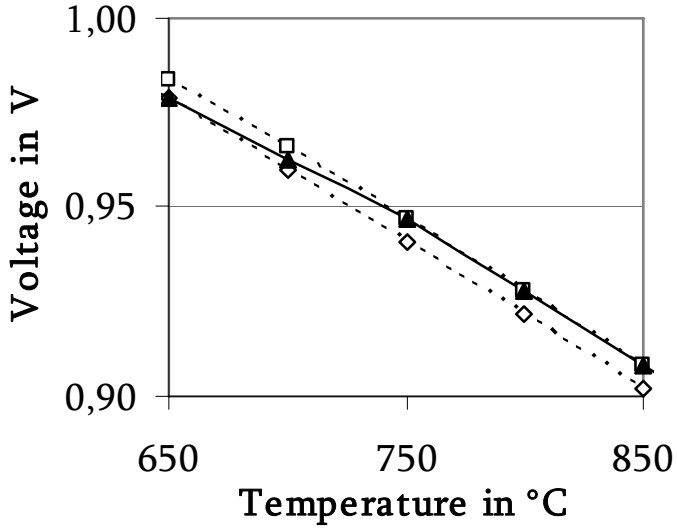


*Figure 2: Theoretical Nernst voltage for 13%CO, 13%$CO_2$, 21%$H_2$, 40%$H_2O$, 1500ppm naphthalene and rest $N_2$. Upper dotted Curve = Equilibrium of hydrocarbons for all temperatures; Bottom dotted Curve = no reforming of Hydrocarbons; black curve = temperature depending reforming [19]*

This paper shows thermodynamical equilibrium calculations for a producer gas from biomass gasification with different tar species of each 5000ppm in order to determine the maximum theoretically achievable OCV for tar laden wood gases. The thermodynamic equilibrium of the reforming process depending on temperature and $H_2O$ content determines the hydrogen and carbon monoxide partial pressure. These effects are extended to the behaviour of the fuel utilization, assuming only hydrogen and carbon monoxide being the fuel. The oxygen partial pressure difference is used to obtain the OCV and the Nernst voltage in operation respectively.

# 1. Scientific Approach

**Producer gas concentrations**
The equilibrium calculations are realised with $H_2$, CO, $CO_2$, $CH_4$, $N_2$ and $H_2O$ which are the main gas components found in biomass gasifiers [17]. The selection of the investigated hydrocarbons aims to cover at least one representing tar species of each tar category. The classification system of [18] includes five classes based on the behaviour of the tar compounds in downstream processes. A list of emerging tars are published in [3] for a fluidised bed gasifier. Table 1 shows the selected tar compounds.

*Table 1: Selection of investigated tar compounds*

| Class | Tar | Concentration |
|---|---|---|
| 2 | Phenol, $C_6H_6O$ | 5000ppm |
| 3 | Toluene, $C_7H_8$ | 5000ppm |
| | o-Xylol, $C_8H_{10}$ | 5000ppm |
| 4 | Naphtalene, $C_{10}H_8$ | 5000ppm |
| 5 | no representitive | |
| - | Benzene, $C_6H_6$ | 5000ppm |

Regarding the classification system, benzene is not considered a tar. Nevertheless, it significantly amounts to the total amount of hydrocarbons present in the product gas.

**Equilibrium Calculation**
The equilibrium calculations based on the minimum Gibbs energy are performed with different tar concentrations, steam contents and temperatures. 228 possible gaseous, liquid and solid products of the reaction mechanisms are considered by the thermodynamic calculation software FactSage 6.0. Ideal gas behaviour is taken into account. Hydrocarbons up to $C_{20}H_y$ are chosen to be considered by the software. Inhibitions of the equilibrium reactions due to kinetics are not considered. Two equilibrium calculations are needed to obtain the OCV and the Nernst voltage in operation respectively. First the equilibrium calculation is applied to the gas concentration as coming from the gasifier in order to obtain the OCV. For the Nernst voltage in operation the amount of oxygen that diffuses from the cathode to the anode side depending on the fuel utilization is added to the equilibrium concentration obtained before for the OCV in order to calculate a new equilibrium concentration. This signifies that the oxygen partial pressure increases at the anode side. The impact on the Nernst voltage due to the decrease of the oxygen partial pressure at the cathode side is not considered.

Different reforming rates for varying $H_2O$ contents and temperatures are aimed at. The equilibrium is looked at for a reforming rate of 0, 20, 40, 60, 80 and 100% for a tar mix as

found in table 1. Especially the necessary amount of $H_2O$ in order to ensure complete reforming and avoid carbon deposition is from particular interest.

**Nernst voltage**

Following derivation explains the calculation of the Nernst voltage using the oxygen partial pressure difference between cathode and anode. In the case of oxidation of hydrogen the equilibrium constant for the anode side can be written ([19], [22]):

$$K_{anode} = \frac{p_{H_2O,anode} \cdot p_0^{\frac{1}{2}}}{p_{H_2,anode} \cdot p_{O_2,anode}^{\frac{1}{2}}} \tag{1}$$

$$\frac{p_{H_2O,anode}}{p_{H_2,anode}} = K_{anode} \frac{p_{O_2,anode}^{\frac{1}{2}}}{p_0^{\frac{1}{2}}} \tag{2}$$

To calculate the Nernst voltage following equation can be used:

$$U_N = -\frac{\Delta^{R,H_2}G(T)}{n_{el} \cdot F} - \frac{R \cdot T}{n_{el} \cdot F} ln\left( \frac{p_{H_2O,anode} \cdot p_0^{\frac{1}{2}}}{p_{H_2,anode} \cdot p_{O_2,cathode}^{\frac{1}{2}}} \right) \tag{3}$$

Putting equation 2 into equation 3 and using,

$$ln(K) = -\frac{\Delta^{R,H_2}G(T)}{R \cdot T} \tag{4}$$

an equation for the Nernst voltage only using the oxygen partial pressures can be derived as follows:

$$U_N = \frac{R \cdot T}{2 \cdot n_{el} \cdot F} ln\left( \frac{p_{O_2,cathode}}{p_{O_2,anode}} \right) \tag{5}$$

This equation is used in the following calculations to obtain the OCV as well as the Nernst voltage in operation. The behaviour of the voltage due to parameter variation is explained by looking at the oxygen partial pressure at the anode side. This is different in as much as usually the actual fuel such as hydrogen and carbon monoxide is taken to interpret the voltage behaviour.

**Fuel Utilization**

Considering hydrogen and carbon monoxide being the fuel for the fuel cell, the amount of available fuel particularly depends on the reforming rate of the hydrocarbons. Here $CH_4$ is not considered being a fuel for direct electrochemical oxidation processes on the anode in order to only indicate the effect of tars. Therefore the fuel utilization is always based on the conversion of hydrogen and carbon monoxide. However, the oxygen partial pressure is taken to investigate the effects of specific parameter variation. For a fuel cell running on a certain electrical load a change of the anode oxygen partial pressure due to alternating producer gas concentrations and thus varying equilibrium concentrations implies a change of fuel utilization which can irreversibly harm the anode because of Nickel oxidation. The

higher the fuel utilization the more oxygen diffuses from the cathode to the anode leading to higher anode oxygen partial pressures and thus to a lower Nernst voltage.

## 2. Calculation

Figure 3 shows the different steps for the calculation of the equilibrium concentration. At the entry of the anode the gas concentration is defined as follows: 21%$H_2$, 13%CO, 13%$CO_2$, varying percentage of $H_2O$ and rest $N_2$. Each tar species amounts for 5000ppm as shown in table 1. $CH_4$ is not used in the start concentration in order to observe the methane production at low temperatures and thus separate it from the effects of tar reforming. At the cathode entry air is used with 21%$O_2$ and 79%$N_2$. The air composition is considered constant in order to avoid effects due to the decrease of the oxygen partial pressure at the cathode side for high fuel utilizations. The total pressure for both anode and cathode is 1bar for all calculations.

While calculating the equilibrium concentration for the OCV the partial pressures of the oxygen and nitrogen at the cathode side stay constant. Depending on the water content the hydrocarbons at the anode are converted into $H_2$ and CO. Also a very small amount of $O_2$ is produced that enables the calculation of the Nernst voltage according equation 5.

To obtain the Nernst voltage in operation the equilibrium concentration from before is taken and augmented by the amount of oxygen diffusing from the cathode side. The oxygen diffusion flow is given through the fuel utilization and the stoichiometric reactions of $H_2$ and CO to $H_2O$ and $CO_2$. Consequently the new equilibrium concentration can be found.

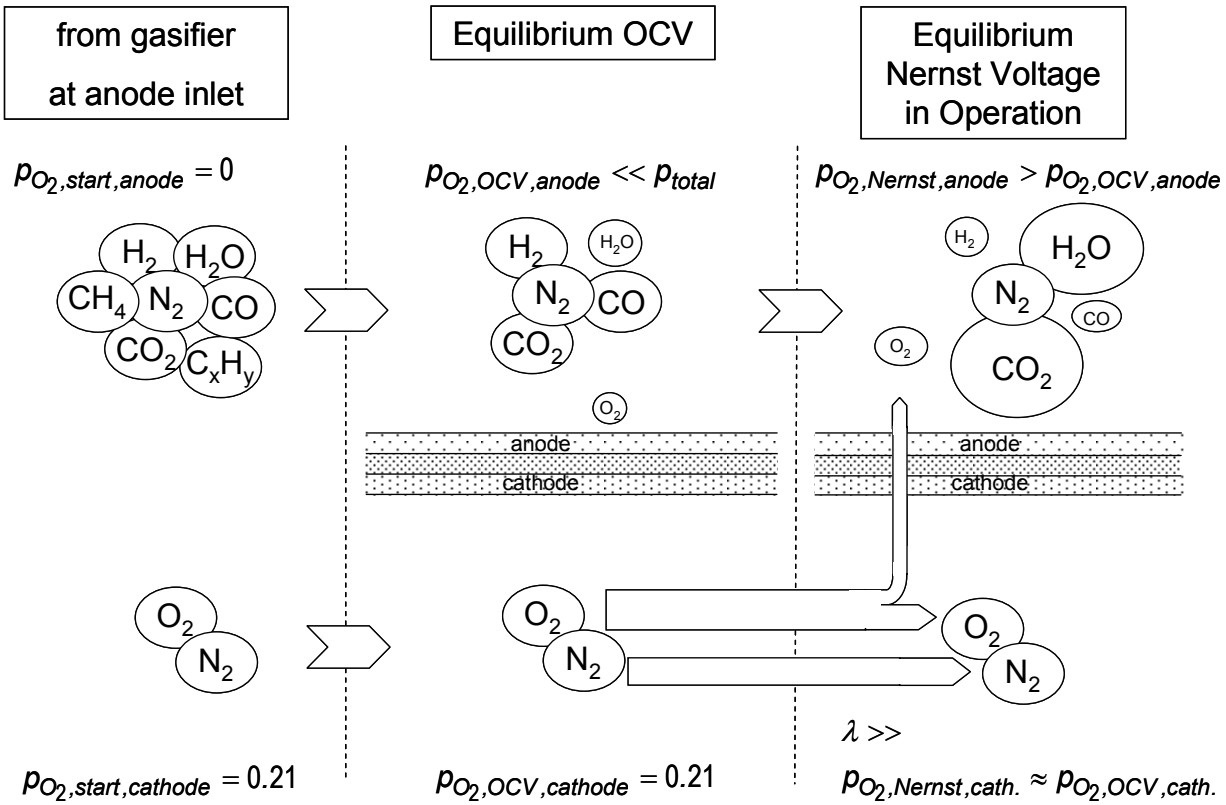


*Figure 3: Model for the stepwise calculation of the equilibrium concentration to gain OCV and Nernst voltage in operation (a high value of the air ratio λ indicates the consideration of a constant air composition)*

The idea of the model is to simulate different reforming rates of the tars between 0 and 100%. Since there is no possibility to partly suppress the reforming reaction within the equilibrium calculation simply the start concentration of the tar mix was changed accordingly. For example having an individual tar concentration of 5000ppm and aiming to simulate 60% reforming leads to an individual tar concentration of 3000ppm. These 3000ppm are taken to calculate the equilibrium while the remaining 2000ppm are balanced by $N_2$. This is important when explaining a lower carbon deposition limit for lower reforming rates later on. In reality a lower reforming rate signifies a certain amount of hydrocarbons to be unconverted. This amount could still lead to carbon deposition whereas in these calculations this effect is not considered due to the use of balance $N_2$.

Furthermore the amount of $H_2O$ and the temperature varies to show their specific impacts to the voltage. For the Nernst voltage during operation the hydrogen and carbon monoxide utilization is used as an additional parameter.

## 3. Results

**OCV: Equilibrium concentration depending on the H2O-content of anode inlet gas**
For the equilibrium calculations a methane free gas is used in order to be able to observe the change of the $H_2$ and CO concentration only due to the reforming of the tars. The tars treated in this study reform completely at temperatures over 873.15K if a sufficient quantity of $H_2O$ is present. Otherwise carbon deposition occurs. Nevertheless, due to the methane reforming reaction,

$$CH_4 + H_2O \leftrightarrow 3H_2 + CO \tag{6}$$

small amounts of methane still will be formed between 873.15 and 1273.15K.

Figure 4 shows a typical equilibrium concentration of 1mol gas mixture containing 21%$H_2$, 13%CO, 13%$CO_2$, 0 to 50%$H_2O$ and rest $N_2$ at 873.15K. There were no methane or higher hydrocarbons present in the initial concentration in order to avoid reforming reactions and thus show the influence of the $H_2O$ content on the oxygen partial pressure. As shown in equation 5 the oxygen partial pressure difference between anode and cathode determines the Nernst voltage. The more $H_2O$ is transported in the initial feed the higher the oxygen partial pressure results for the equilibrium concentration. In the region of low $H_2O$ contents the Boudouard reaction is responsible for carbon deposition.

The increasing $H_2O$ content leads to a linear decrease of the solid carbon due to following reactions:

$$C + H_2O \rightarrow CO + H_2 \tag{7}$$
$$CO + H_2O \rightarrow CO_2 + H_2 \tag{8}$$

Therefore the amount fractions of $H_2$, CO and $CO_2$ also increase linearly. At $H_2O$ concentrations above the carbon deposition limit the production of CO due to equation 7 stops leading to a diminishing CO concentration. In the same way the production of $H_2$ and $CO_2$ becomes less. The rising oxygen partial pressure deduces from the following reaction:

$$H_2 + \frac{1}{2}O_2 \leftrightarrow H_2O \tag{9}$$

Even though the equilibrium for this reaction strongly tends to the right small amounts of oxygen are present in the equilibrium concentration. The oxygen amount fraction can be seen in figure 4 (right graph) on the right vertical axis. A linear gradient in the area of carbon deposition is observed. At higher $H_2O$ levels the equilibrium of reaction 9 is slightly more forced to the left.

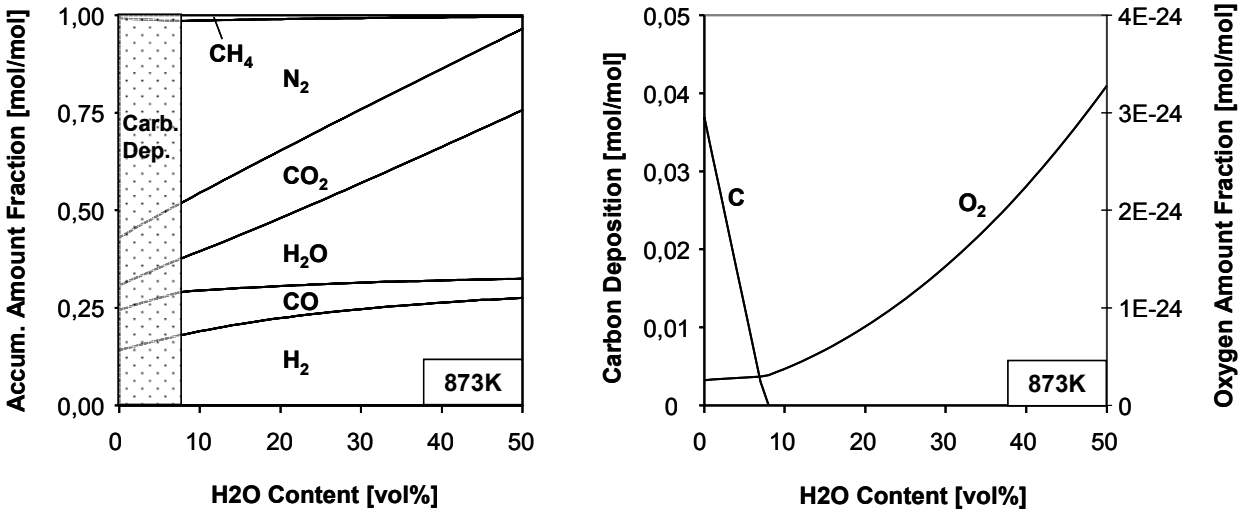


*Figure 4: Equilibrium Concentrations for an anode inlet gas containing 21%$H_2$, 13%CO, 13%$CO_2$, 0-50% $H_2O$ and rest $N_2$. Left graph: Accumulated amount fractions. Right graph: amount of carbon deposition in [mol C/mol anode inlet gas] and oxygen amount fraction in [mol /mol]*

This change of gradient due to the carbon deposition limit becomes more obvious on a logaritmic scale as shown in figure 5. The six lines of each graph show the equilibrium oxygen partial pressures at 873.15, 1073.15 and 1273.15K for an anode inlet gas with the same $H_2$, CO, $CO_2$, $H_2O$ and $N_2$ concentration as described before. The six curves only differ from each other in terms of their reforming rate. An individual tar load of 5000ppm for naphthalene ($C_{10}H_8$), o-xylol ($C_8H_{10}$), toluene ($C_7H_8$), phenol ($C_6H_6O$) and benzene ($C_6H_6$) is applied. The reforming rate is stepwise increased from 0 up to 100% in 20% steps. Since the unconverted amount of tar below reforming rates of 100% is considered to be inert less carbon for carbon deposition is present the lower the reforming rate is. Due to the reforming reaction,

$$C_xH_y + xH_2O \rightarrow \left(x + \frac{y}{2}\right)H_2 + xCO \qquad (10)$$

more $H_2$ and CO is produced at higher $H_2O$ levels. Also the equilibrium for reaction 9 is pushed more to the right leading to a smaller oxygen partial pressure. According to equation 5 a smaller anode oxygen partial pressure generates a higher Nernst voltage. This goes along with the assumption that reforming higher hydrocarbons provides more fuel in form of $H_2$ and CO. Due to the Boudouard reaction more carbon is built at lower temperatures which can be seen in figure 5 from the point indicated with an arrow illustrating both the gradient change of the oxygen partial pressure and the carbon deposition limit. Lower temperatures push the equilibrium of reaction 9 more to the right explaining a general lower oxygen partial pressure. This confirms the theory of decreasing Nernst voltages with increasing temperatures using equation 5.

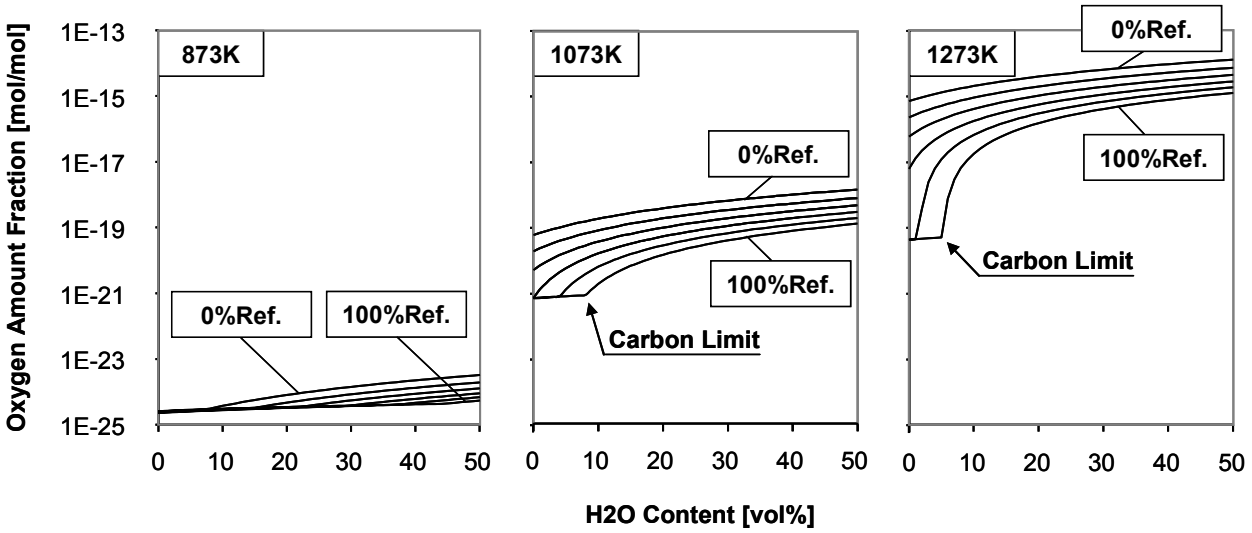


*Figure 5: Oxygen amount fraction for an anode inlet gas containing 21%$H_2$, 13%CO, 13%$CO_2$, 0-50% $H_2O$ and rest $N_2$ at 873.15 (left), 1073.15 (middle) and 1273.15K (right). The six curves represent 0 to 100% reformation in 20% steps. The individual tar contents for $C_{10}H_8$, $C_8H_{10}$, $C_7H_8$, $C_6H_6O$ and $C_6H_6$ of the inlet gas are 5000ppm.*

Figure 6 transfers the behaviour of the oxygen partial pressure depending on temperature, reforming rate and H2O content into the OCV for a fuel cell. Three couples of curves showing the trend of the OCV are drawn for 873.15, 1073.15 and 1273.15K. Again the anode inlet gas concentration contains 21%$H_2$, 13%CO, 13%$CO_2$, 0 to 50%$H_2O$ and rest $N_2$. For the cathode side air (21%$O_2$ and 79%$N_2$) is used. Due to equation 5 the oxygen partial pressure at the cathode side significantly determines the Nernst voltage. For each temperature the OCV for the anode inlet gas with 5000ppm individual tar load is compared for 0 and 100% reforming rate. The comparison shows the potential voltage increase due to the reforming of hydrocarbons. In the region of carbon deposition the OCV progresses linearly similar to the oxygen partial pressure as shown in figure 4 and 5.

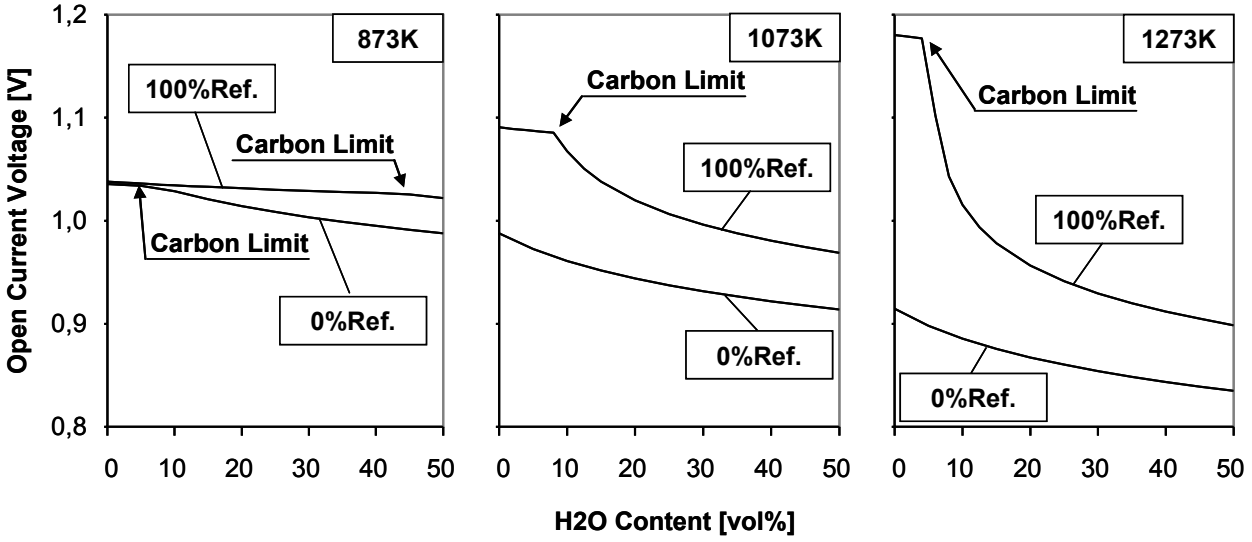


*Figure 6: OCV for an anode inlet gas containing 21%$H_2$, 13%CO, 13%$CO_2$, 0-50% $H_2O$ and rest $N_2$ at 873.15 (left), 1073.15 (middle) and 1273.15K (right) for 0 and 100% reforming rate. The individual tar contents for $C_{10}H_8$, $C_8H_{10}$, $C_7H_8$, $C_6H_6O$ and $C_6H_6$ of the inlet gas are 5000ppm.*

**OCV: Equilibrium concentration depending on the temperature of anode inlet gas**

The temperature dependency on the OCV is explained in figure 7. The six full curves represent the OCV over the temperature with reforming rates between 0 and 100% in 20% steps. The anode inlet gas contains 21%$H_2$, 13%CO, 13%$CO_2$, 45%$H_2O$ with rest $N_2$. 45%$H_2O$ is chosen in order to avoid carbon deposition for all different reforming rates even at 873.15K. The potential voltage increase due to reforming becomes evident when comparing the curve for a fully reformed gas with the curve for a non reformed gas.

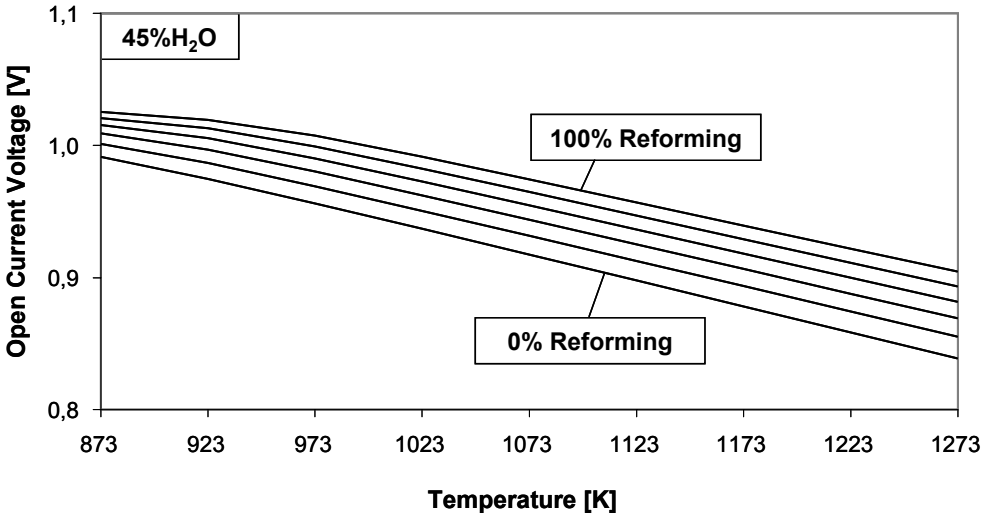


*Figure 7: OCV for an anode inlet gas containing 21%$H_2$, 13%CO, 13%$CO_2$, 45%$H_2O$ and rest $N_2$ for 0, 20, 40, 60, 80 and 100% reforming rate. The individual tar contents for $C_{10}H_8$, $C_8H_{10}$, $C_7H_8$, $C_6H_6O$ and $C_6H_6$ of the inlet gas are 5000ppm.*

As can be seen in figure 5 lowest oxygen partial pressures can be achieved close to the carbon deposition limit. Thus the highest OCV for each temperature that can be achieved by adding only as much $H_2O$ as is needed to prevent carbon deposition is an interesting parameter for optimal gas conditioning for fuel cells. For eight indicated points the OCV is calculated in figure 8 for 100% reforming. The upper curve shows that the higher the temperature is the less $H_2O$ is needed to avoid carbon deposition due to the Boudouard reaction. At a temperature of about 1073.15K the limit of $H_2O$ reduction is reached since carbon deposition would appear due to decomposition of hydrocarbons. The bottom curve represents the OCV for the case of a constant $H_2O$ content of 45% along the whole temperature range. The less excess $H_2O$ is available the smaller the oxygen partial pressure will be and thus the OCV increases. These curves show the significance of an appropriate humidification of the anode inlet gas.

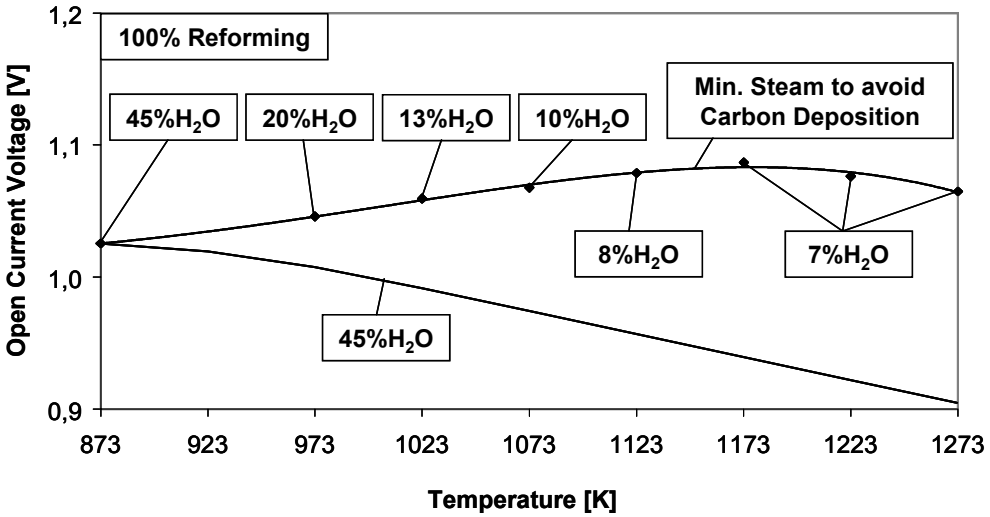


*Figure 8: Bottom curve: OCV for an anode inlet gas containing 21%$H_2$, 13%CO, 13%$CO_2$, 45% $H_2O$ and rest $N_2$. The individual tar contents for $C_{10}H_8$, $C_8H_{10}$, $C_7H_8$, $C_6H_6O$ and $C_6H_6$ of the inlet gas are 5000ppm. Upper curve: same inlet gas concentration but with only as much $H_2O$ as needed to avoid carbon deposition.*

**OCV: Equilibrium concentration depending on the reforming rate of anode inlet gas**

Figure 9 shows various curves for the OCV depending on the reforming rate for 873.15, 1073.15 and 1273.15K. The bottom curves always represent the OCV for a constant $H_2O$ content of 45, 9 and 6% respectively. The upper curves show the OCV with only as much $H_2O$ as it is necessary for the specific reforming rate to avoid carbon deposition. Thus the potential of the OCV due to an appropriate amount of $H_2O$ again becomes evident when looking at the curves for a constant level of $H_2O$ and the ones with a carbon prevention depending $H_2O$ content. The 45, 9, and 6% $H_2O$ content result from the most critical point for carbon deposition at the respective temperature for 5000ppm individual tar concentration. This is always where the two curves meet. The OCV for the upper curves is higher because less $H_2O$ is present and furthermore less oxygen is produced at equilibrium.

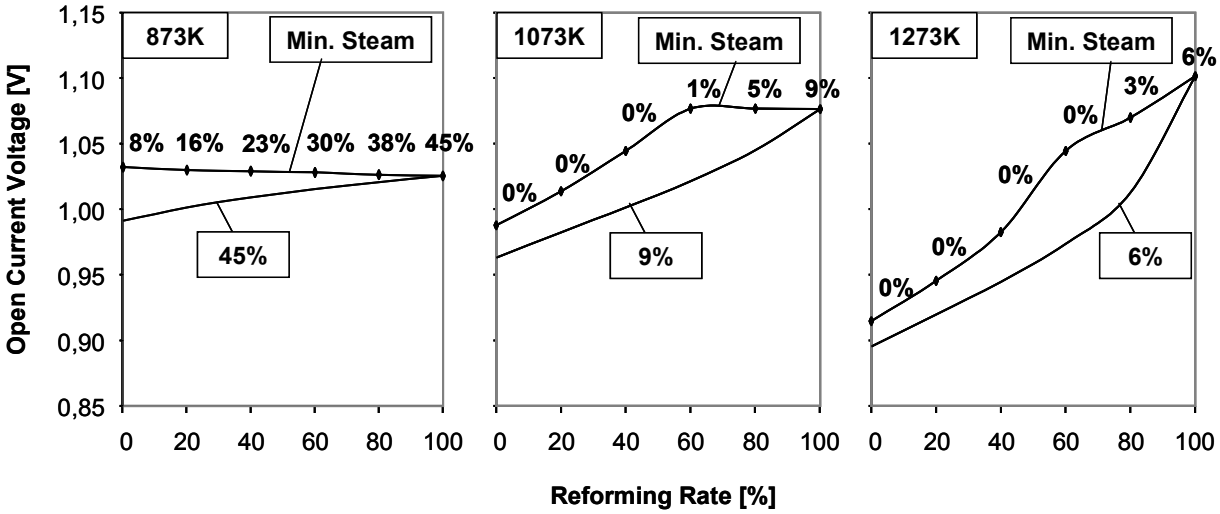


*Figure 9: OCV for an anode inlet gas containing 21%$H_2$, 13%CO, 13%$CO_2$, and rest $N_2$ at 873.15 (left), 1073.15 (middle) and 1273.15K (right). The individual tar contents for $C_{10}H_8$, $C_8H_{10}$, $C_7H_8$, $C_6H_6O$ and $C_6H_6$ of the inlet gas are 5000ppm. Bottom curves: OCV for inlet gas containing 45, 9 and 6%$H_2O$ respectively for the whole range. Upper curves: OCV with just as much $H_2O$ as it is necessary to prevent carbon formation.*

**$H_2$/CO utilization and Nernst voltage in operation**

Figure 10 shows the hydrogen and carbon monoxide utilization as well as the Nernst voltage depending on the reforming rate for 1073.15K and 10%$H_2O$. To calculate the Nernst voltage under a certain electrical load the oxygen flow due to the stoichiometric electrochemical oxidation of $H_2$ and CO is determined. The resulting amount of oxygen is put to the equilibrium concentration gained from the OCV calculations as explained in chapter 2. Once more the equilibrium concentration is obtained and the Nernst voltage in operation can be calculated using equation 5.

The upper curve of the left graph and the bottom curve of the right graph in figure 10 represent the $H_2$/CO utilization and the Nernst voltage respectively for the case that 85% of the hydrogen and carbon monoxide present in the OCV equilibrium concentration becomes oxidized. Therefore the amount of oxygen that is needed to oxidize 85% of $H_2$ and CO is added to obtain the new equilibrium concentration. This oxygen amount defines the current density needed to achieve a $H_2$/CO utilization of 85%. The real $H_2$/CO utilization slightly differs from 85% because not all the oxygen is used for the $H_2$/CO oxidation according to the equilibrium. The value for the Nernst voltage increases almost linearly. Since the anode oxygen partial pressure increases with higher electrical loads and oxygen diffusion flows through the membrane respectively the Nernst voltage shrinks compared to the OCV as shown in the middle graph of figure 9.

In the second case the oxygen diffusion flow and current density resulting from 85% $H_2$/CO utilization for 0% reforming is kept constant while increasing the reforming rate. This is equivalent to a constant current density. With an increasing reforming rate more $H_2$ and CO is built from the reforming reactions leading to lower oxygen partial pressures. Hence, the Nernst voltage starts to increase as can be seen from the upper curve in the right graph. Since the oxygen diffusion flow is constant the amount of $H_2$ and CO that is oxidized stays constant too leaving more $H_2$ and CO unused. This can be seen by the bottom curve in the left graph for the $H_2$/CO utilization showing lower values at higher reforming rates.

This observation is significant for the operation of fuel cells with biogenious gases from gasification. Simply the differences in the quality of the biomass feed, e.g. the water content, can cause fluctuations in the gas concentration. Varying tar concentrations therefore can quickly lead to changes of the fuel utilization and cell voltage. Furthermore the risk of reaching too high $H_2$/CO utilizations exists when the tar concentration diminishes. High $H_2$/CO utilizations signify a high oxygen partial pressure at the anode side which can cause Nickel oxidation.

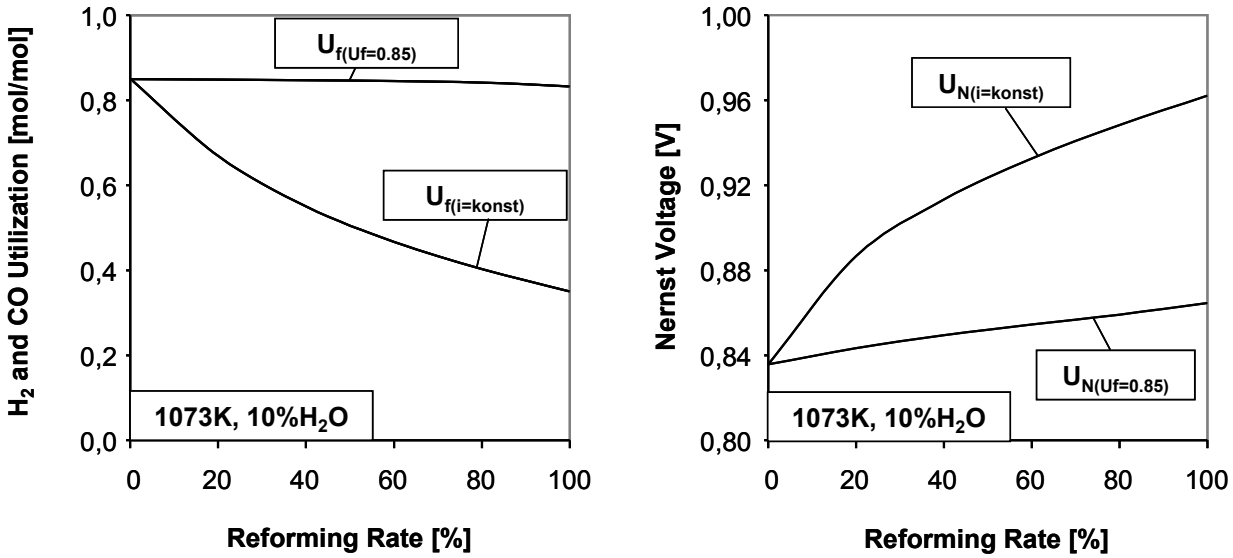


*Figure 10: $H_2$ and CO utilization (left) and Nernst voltage (right) for an anode inlet gas containing 21%$H_2$, 13%CO, 13%$CO_2$, 10% $H_2O$ and rest $N_2$ at 1073.15K for constant H2/CO utilization and constant current density. The individual tar contents for $C_{10}H_8$, $C_8H_{10}$, $C_7H_8$, $C_6H_6O$ and $C_6H_6$ of the inlet gas are 5000ppm.*

Figure 11 combines the effect of different reforming rates and changes in $H_2$/CO utilization. The upper left graph shows the Nernst voltage in operation for 0 and 100% reforming over the current density. With an increasing reforming rate more $H_2$ and CO can be oxidized. Therefore the maximum possible oxygen diffusion flow and thus the current density increases. This can be seen by the upper curve going far more towards higher current densities. The upper right graph again represents the Nernst voltage but over the $H_2$/CO utilization. Similar to the right graph in figure 10 the reforming rate over the $H_2$/CO utilization is shown in the bottom right graph of figure 11. There a constant current density of the same value as it is indicated through the vertical dotted line in the upper left graph at $i_{max,0\%ref.}$ is used. The current density $i_{max,0\%ref.}$ is achieved at 85% $H_2$/CO utilization and 0% reforming.

Keeping the $H_2$/CO utilization at 85% but having 100% reforming instead of 0% increases the Nernst voltage indicated by $\Delta U_{N,U\_H2/CO=const.}$ in the upper right graph. Furthermore the increase of the current density is shown in the upper left graph named $\Delta i_{max}$.

For a constant current density of $i_{max,0\%ref.}$ the increase of the Nernst voltage between the two cases of 0 and 100% reforming can be seen by $\Delta U_{N,i=const.}$. This increase of the reforming rate leads to a decrease of the $H_2$/CO utilization from 85% down to 35%. The change of the H2/CO utilization is shown through $\Delta U_{H2/CO}$.

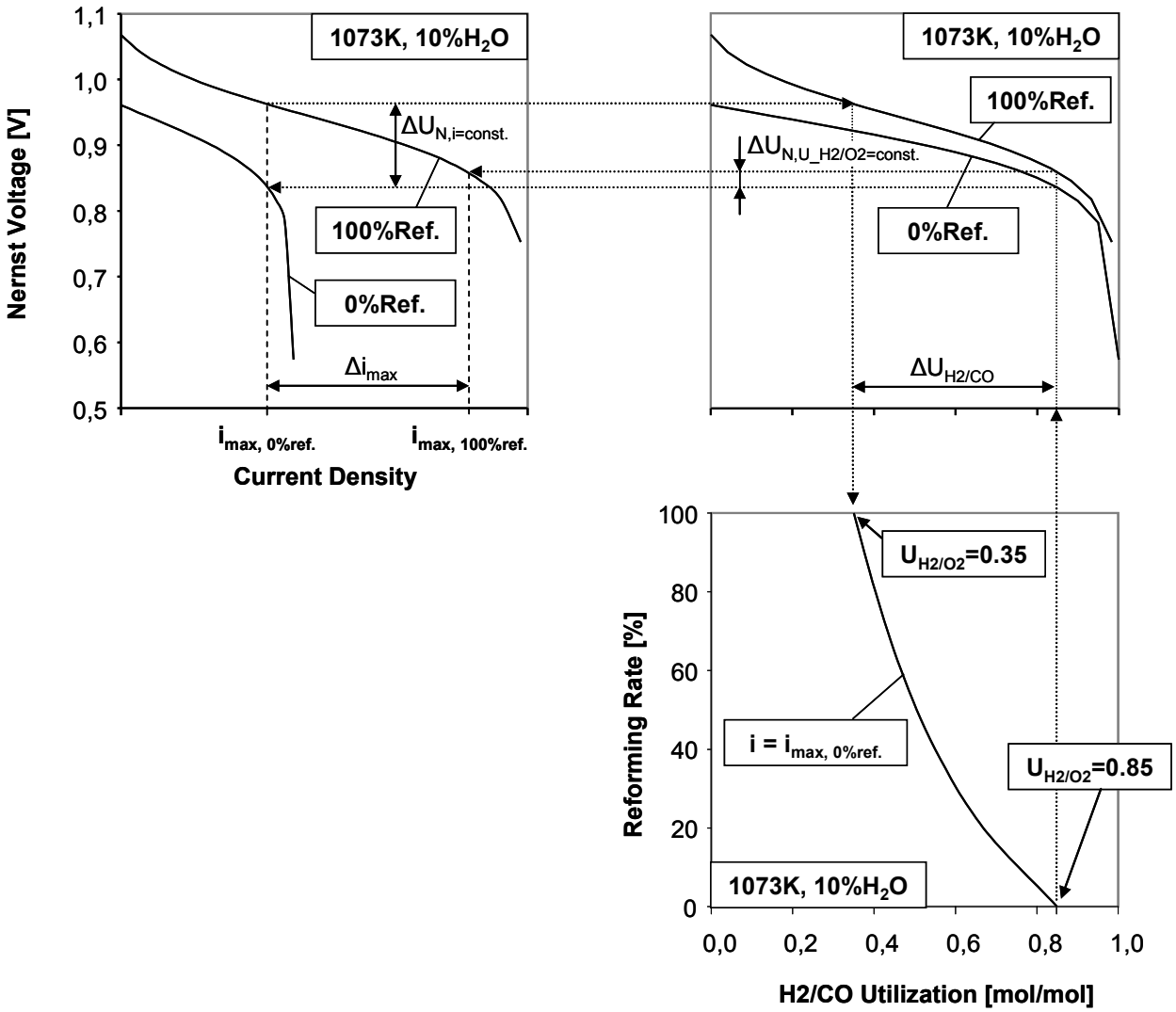


*Figure 11: Nernst voltage depending on current density (upper left) and $H_2$/CO utilization (upper right) and reforming rate depending on $H_2$/CO utilization (bottom right) for an anode inlet gas containing 21%$H_2$, 13%CO, 13%$CO_2$, 10% $H_2O$ and rest $N_2$ at 1073.15K. The individual tar contents for $C_{10}H_8$, $C_8H_{10}$, $C_7H_8$, $C_6H_6O$ and $C_6H_6$ of the inlet gas are 5000ppm. ($i_{max,0\%ref.}$: maximum current density for 85% $H_2$/CO utilization and 0% reforming, $i_{max,100\%ref.}$: maximum current density for 85% $H_2$/CO utilization and 100% reforming)*

Using these graphs the effects on the Nernst voltage are pictured. These effects further directly influence the real cell voltage which is the Nernst voltage diminished by activation, ohmic and concentration polarization.

## 4. Conclusion

The use of biogenious gases from biomass gasification in SOFCs depicts a promising technology. A big challenge is to handle the gas impurities without substantially reducing the system efficiency. One main aspect is the conversion of higher hydrocarbons, so called tars. Recent results from experiments have shown a high tolerance of SOFCs against such gas impurities ([3], [19]). The Nickel anode of an SOFC provides catalytic properties enabling reforming of tars directly on the anode surface. Therefore tars can be seen as an additional fuel. In [19] the potential voltage increase due to naphthalene, methane, toluene and phenol is described.

This paper shows the dependency of the voltage for different reforming rates at varying $H_2O$ contents and temperatures. Several reforming rates are considered for a tar mix assuming equilibrium at the anode. The Open Current Voltage as well as the Nernst voltage in operation gives information about the potential voltage increase due to reforming of tars. These effects are further outlined by showing the hydrogen and carbon monoxide utilization during changing reforming rates. High $H_2$/CO utilizations mean high oxygen partial pressures that furthermore promote nickel oxidation of the anode.

These calculations are the basis for single cell tests of planar SOFCs with synthetic and real wood gas. It is intended to track the influence of several representative tar species. A comparison between the theoretic equilibrium voltage and the real measured voltage is expected to explain the behaviour of tar reforming at the anode.

## References

(1) Karl J., Karellas S.; Highly efficient SOFC systems with indirect gasification. In: Proceedings of the 6th European Solid Oxide Fuel cell Forum, Vol. 2, pages 534-545, Lucerne, Switzerland, June 2004
(2) Schweiger A., Hohenwarter U., Karl J.; Verstromung von Biomasse – Produktgasen in Solid Oxide Fuel Cells. 9. Symposium Energieinnovation, Graz, Austria, February 2006
(3) A. Schweiger; Heissgasreinigung. Dissertation, Graz, Austria, 2008
(4) J.O. Ouweltjes; Degradation mechanisms - Influence of hydrocarbons. BioCellus Summer School, Seggau, Austria, 2007
(5) Saule M., Frank N., Hofmann P., Ouweltjes J. P., Schweiger A., Karl J.; Operation of Solid Oxide Fuel Cells with Syngas from Biomass. H2expo, Hamburg, Germany, 2006
(6) Saunders G.J., Kendall K.; Reactions of hydrocarbons in small tubular SOFCs. Journal of Power Sources 106 (2002) 258-263
(7) Laosiripojana N., Sangtongkitcharoen W., Assabumrungrat S.; Catalytic steam reforming of ethane and propane over CeO2-doped Ni/Al2O3 at SOFC temperature: Improvement of resistance toward carbon formation by the redox property of doping CeO2. Fuel 85 (2006) 323-332
(8) Kim T., Liu G., Boaro M., Lee S.-I., Vohs J.M., Gorte R.J., Al-Mahdi O.H., Dabbousi B.O.; A study of carbon formation and prevention in hydrocarbon-fuelled SOFC. Journal of Power Sources 155 (2006) 231-238
(9) Klein J.-M., Bultel Y., Georges S., Pons M.; Modeling of a SOFC fuelled by methane: From direct internal reforming to gradual internal reforming. Chemical Engineering Science 62 (2007) 1636-1649
(10) Laosiripojana N., Assabumrungrat S.; Catalytic steam reforming of methane, methanol, and ethanol over Ni/YSZ: The possible use of these fuels in internal reforming SOFC. Journal of Power Sources 163 (2007) 943-951
(11) Xu, J., Froment, G.; Methane Steam Reforming, Methanisation and Water-Gas Shift: I. Intrinsic Kinetics. AIChE Journal, 35 (1989) [1] S.88-96
(12) Shekhawat D., Berry A.D., Haynes J.D., Spivey J.J.; Fuel constituent effects on fuel reforming properties for fuel cell applications. Fuel 88 (2009) 817-825
(13) Jess A.; Catalytic upgrading of tarry fuel gases: A kinetic study with model components. Chemical Engineering and Processing 35 (1996) 487-494
(14) Jess A.; Mechanisms and kinetics of thermal reactions of aromatic hydrocarbons from pyrolysis of solid fuels. Fuel Vol.75, No.12, pp. 1441-1448, 1996

(15) Depner H., Jess A.; Kinetics of nickel-catalyzed purification of tarry fuel gases from gasification and pyrolysis of solid fuels. Fuel 78 (1999) 1369-1377
(16) Biomass Gasification – Tar and Particles in Product Gases – Sampling and Analysis. CEN/BT/TF 143, TC BT/TF 143 WICSC 03002.4:2004(E), 2004/10
(17) Schweiger A., Hohenwarter U.; Small scale hot gas cleaning device for SOFC utilization of woody biomass product gas. 15th European Biomass Conference & Exhibition ICC International Congress Center Berlin, Germany, 2007
(18) van Paasen S.V.B, Kiel J.H.A.; Tar formation in fluidised-bed gasification – Impact of gasifier operating conditions. 2nd World Conference and Technology Exhibition on Biomass for Energy, Industry and Climate Protection, Rome, Italy, May 2004
(19) Frank, N.; Umsetzung von Teeren in SOFCs. Dissertation, Munich, Germany, 2009
(20) J. Karl, S. Karellas, N. Frank, H. Spliethoff; Highly efficient conversion of syngas from biomass gasification in Solid Oxide Fuel Cells,14th European Conference and Technology
(21) W. Santongkitcharoen, S. Assabumrungrat, V. Pavarajarn, N. Laosiripojana, P. Praserthdam; Comparison of carbon formation boundary in different modes of Solid Oxide Fuel Cells fueled by methane. Journal of Power Sources 142 (2005) 75-80
(22) McIntosh, S., Gorte, R.J.; Direct Hydrocarbon Solid Oxide Fuel Cells. Chem. Rev. 2004 (104) S.4845-4865